Journal of Alloys and Compounds 504 (2010) 129–133

Contents lists available at ScienceDirect

Journal of Alloys and Compounds

journal homepage: www.elsevier.com/locate/jallcom

Ferro-piezoelectric properties of $0.94(Na_{0.5}Bi_{0.5})TiO_3$–$0.06BaTiO_3$ thin film prepared by metal–organic decomposition

D.Z. Zhang[a], X.J. Zheng[a,b,*], X. Feng[c], T. Zhang[d], J. Sun[a], S.H. Dai[a], L.J. Gong[a,b], Y.Q. Gong[a,b], L. He[a,b], Z. Zhu[a], J. Huang[a], X. Xu[a]

[a] Faculty of Materials, Optoelectronics and Physics, Xiangtan University, Xiangtan, Hunan 411105, PR China
[b] Key Laboratory of Low Dimensional Materials and Application Technology of the Ministry of Education, Xiangtan University, Xiangtan, Hunan 411105, PR China
[c] School of Aerospace, Tsinghua University, Beijing 100084, PR China
[d] Department of Electronic Engineering, Jilin University, Changchun, Jilin 130012, PR China

ARTICLE INFO

Article history:
Received 8 December 2009
Received in revised form 13 May 2010
Accepted 21 May 2010
Available online 1 June 2010

Keywords:
Thin films
Ferroelectrics
Crystal growth
Piezoelectricity

ABSTRACT

$0.94(Na_{0.5}Bi_{0.5})TiO_3$–$0.06BaTiO_3$ thin film was fabricated by metal–organic decomposition, and the butterfly-shaped piezoelectric response curve was measured by a scanning probe microscopy system. The remanent polarization $2P_r$ and coercive field E_c are 24 μC/cm^2 and 103 kV/cm under 782 kV/cm, and the dielectric constant and dielectric loss are 504 and 0.05 at 1 kHz. The average values of effective piezoelectric coefficient d^*_{33} and electrically induced strain are 94 pm/V and 0.3% under the bipolar driving field of 391 kV/cm, and the mechanisms concerning the dependence of the high piezoelectric properties were also discussed.

1. Introduction

Piezoelectric $Pb(Zr,Ti)O_3$ (PZT) is widely used in micro-electro-mechanical systems (MEMS), microactuators, transducers, micromotors and strain gauges due to the superior piezoelectric properties [1]. The lead toxicities of producing, using and recycling are problematic for devices associated with PZT and other lead oxide-based piezoelectrics, therefore lead-free piezoelectric materials are desired inevitably as candidate materials in place of PZT for the sake of environmental protection and biocompatibility [2]. Among various lead-free piezoelectric materials $(Na_{0.5}Bi_{0.5})TiO_3$ (NBT) ceramic is recognized as one of key materials because of its relatively large ferroelectric properties at room temperature [3]. However, pure NBT suffers from its high conductivity and large coercive field, making it difficult to obtain the desired properties [4]. To solve this problem, varieties of NBT-based solid solutions, such as NBT–$BaTiO_3$ [4–6], NBT–$SrTiO_3$ [7], NBT–$YMnO_3$ [8], NBT–$Bi_{0.5}K_{0.5}TiO_3$ [9] and NBT–$Ba_{0.7}Sr_{0.3}TiO_3$ [10], have been developed. In contrast with pure NBT, the NBT-based solid solutions show the improved ferroelectric, dielectric and piezoelectric properties. Among them $(1-x)(Na_{0.5}Bi_{0.5})TiO_3$–$xBaTiO_3$(NBT–BT$x$) solid solution with a composition near rhombohedral–tetragonal morphotropic phase boundary (MPB, about $x = 0.06$) has attracted considerable attention on account of the high piezoelectric properties [6,11–13]. Generally, single crystal and ceramic of NBT–BTx are focused on the ferroelectric, dielectric and piezoelectric properties [4–6,11–14]. However the NBT–BTx thin film is only focused on the ferroelectric and dielectric properties [15–17], and is seldom involved in the piezoelectric performance. Piezoelectric materials, especially in form of thin film, offer a number of advantages in MEMS, such as low hysteresis, high available energy density, high sensitivity with wide dynamic range, and low power requirement, therefore it is worth considering the impetus for integrating piezoelectric thin films into MEMS devices [18]. Nevertheless, one of the major problems in the design and fabrication of piezoelectric-based MEMS is that piezoelectric and electrostriction coefficients that determine the electromechanical strain of microactuators and sensitivity of microsensors are poorly investigated in typical film piezoelectrics [19].

Because NBT–BTx single crystal and ceramic show high piezoelectric performance near MPB [6,11–13], we naturally wonder whether NBT–BTx thin film near MPB region is of the high piezoelectric properties. In this study, $0.94(Na_{0.5}Bi_{0.5})TiO_3$–$0.06BaTiO_3$ (NBT–BT6) thin film was fabricated by metal–organic decomposition (MOD) method, and by using a scanning probe microscopy system the butterfly-shaped piezoelectric response curve was

* Corresponding author at: Faculty of Materials, Optoelectronics and Physics, Xiangtan University, Xiangtan, Hunan 411105, PR China. Tel.: +86 731 58293648; fax: +86 731 58298119.
E-mail address: zhengxuejun@xtu.edu.cn (X.J. Zheng).

0925-8388/$ – see front matter © 2010 Elsevier B.V. All rights reserved.
doi:10.1016/j.jallcom.2010.05.069

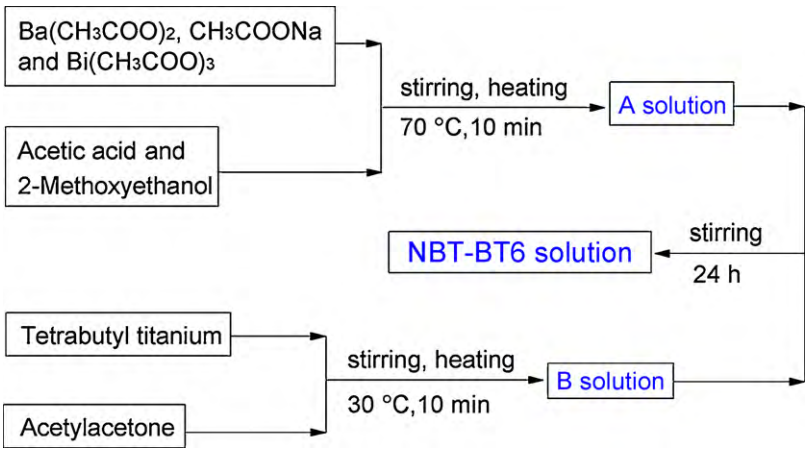

Fig. 1. Flow chart of preparation process for NBT–BT6 precursor solution.

measured to obtain the electrically induced strain and effective piezoelectric coefficient d^*_{33}. The average value of d^*_{33} would be compared with those of PZT thin films and some lead-free piezoelectric thin films, and it is expected that the present research may offer useful guidelines to the design and application of piezoelectric NBT-based thin films.

2. Experimental procedures

NBT–BT6 thin film was grown on Pt/Ti/SiO_2/Si(1 0 0) substrate by MOD method using a repeated coating/drying cycle. Barium acetate ($Ba(CH_3COO)_2$), bismuth acetate ($Bi(CH_3COO)_3$), sodium acetate (CH_3COONa) and tetrabutyl titanium ($Ti(OCH_2CH_2CH_2CH_3)_4$) were used as starting materials for the preparation of NBT–BT6 precursor solution with concentration of 0.2 M. Acetic acid (CH_3COOH) and 2-methoxyethanol ($CH_3OCH_2CH_2OH$) with volume ratio of 1:1 were chosen as co-solvent. The flow chart of synthesis process for NBT–BT6 precursor solution is shown in Fig. 1. During the preparation, the tetrabutyl titanium was at first dissolved in acetylacetone ($CH_3COCH_2COCH_3$) in order to avoid the hydrolysis of tetrabutyl titanium caused by the moisture in air. A 10% excess amount of bismuth acetate was added to compensate for possible Bi loss during high temperature annealing. The mixture of A and B solutions was constantly stirred about 24 h until a transparent and stable yellow precursor solution was obtained. After placing about five days and filtering, the precursor solution was spun on the substrate at 400 rpm for 10 s and 4000 rpm for 40 s, dried at 200 °C for 5 min, and pyrolyzed at 450 °C for 5 min to remove residual organic ingredients. The coating/drying cycle was repeated eight times to gain the desired film thickness. After the eight cycles, the prebaked thin film was annealed at 750 °C for 1200 s in oxygen atmosphere to promote crystallization by rapid thermal annealing process.

Phase identification and crystalline orientation of NBT–BT6 thin film were characterized by an X-ray diffractometer (XRD, D/Max 2550 VB, Rigaku, Japan) with Cu K_α radiation. The chemical composition of the thin film was analyzed by an energy-dispersive X-ray spectroscopy (EDS, INCA, Oxford, England), where the accelerating voltage of EDS electron beam was 20 kV. Surface morphology, grain size and surface roughness of the thin film were identified by an atomic force microscopy (AFM, Nanoscope Multimode NS-3D, DI, USA), and the cross-sectional micrograph and film thickness were obtained by a field emission scanning electron microscopy (FE-SEM, 1525, LEO, Germany). In order to measure ferroelectric and dielectric properties, circular Pt top electrodes with radius of 0.1 mm were deposited on the thin film using a shadow mask by dc magnetron sputtering. The polarization-electric field (P–E) hysteresis loops were measured at the frequency of 1 kHz by a ferroelectric test module (TF 2000 analyzer, axiACCT, Germany) under the various applied voltages in the range of 6–18 V, and the dielectric constant and dielectric loss were measured by an impedance analyzer (HP4194A, Hewlett Packard, USA) in the frequency range of 100 Hz–100 kHz at room temperature. The local piezoelectric properties of the thin film without top electrodes were characterized by a commercially available scanning probe microscopy system (SPM, SPI4000&SPA300HV, Seiko, Japan), which is equipped with a conductive Rh-coated silicon cantilever (SI-DF3, Seiko, Japan) with a spring constant of 1.9 N/m, a resonant frequency of 28 kHz, and an integrated tip of about 10 nm in diameter. A first cycle piezoelectric displacement–voltage (D–V) curve induced by converse piezoelectric effect was recorded by keeping SPM tip fixed on an interesting point of thin film and applying a dc voltage between −9 V and 9 V [20]. Since the intersection of D–V curve has an unexpected shift from the origin, the D–V curve can be converted to a piezoelectric hysteresis ($d^*_{33} - V$) loop via the modified equation of converse piezoelectric effect [21].

$$d^*_{33} = \frac{D - D_I}{V - V_I} \quad (1)$$

As for D–V curve, D and V are piezoelectric displacement and applied voltage for each point, while D_I and V_I are piezoelectric displacement and applied voltage for the intersection. Considering the local method of piezoelectric characterization for SPM [22,23], the first cycle piezoelectric measurement was repeatedly conducted on 29 points within the scanned scope of 300 nm × 300 nm area on thin film surface.

3. Results and discussion

The formation of NBT–BT6 thin film by MOD method can be conceptually divided into two regimes [24]. One corresponds to the decomposition of the metal–organic precursor and to the formation of the inorganic phase by decomposition and solid-state reaction, occurring for the pyrolysis temperature about 450 °C. The second regime corresponds to the crystallization of the inorganic compound by the nucleation and growth of randomly oriented NBT–BT6

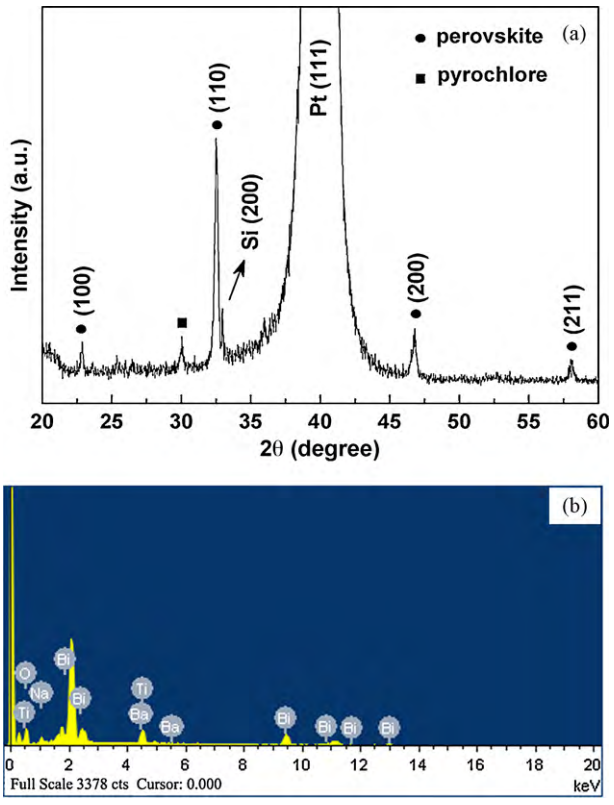

Fig. 2. (a) XRD pattern, and (b) EDS spectrum of NBT–BT6 thin film deposited on Pt/Ti/SiO_2/Si substrate.

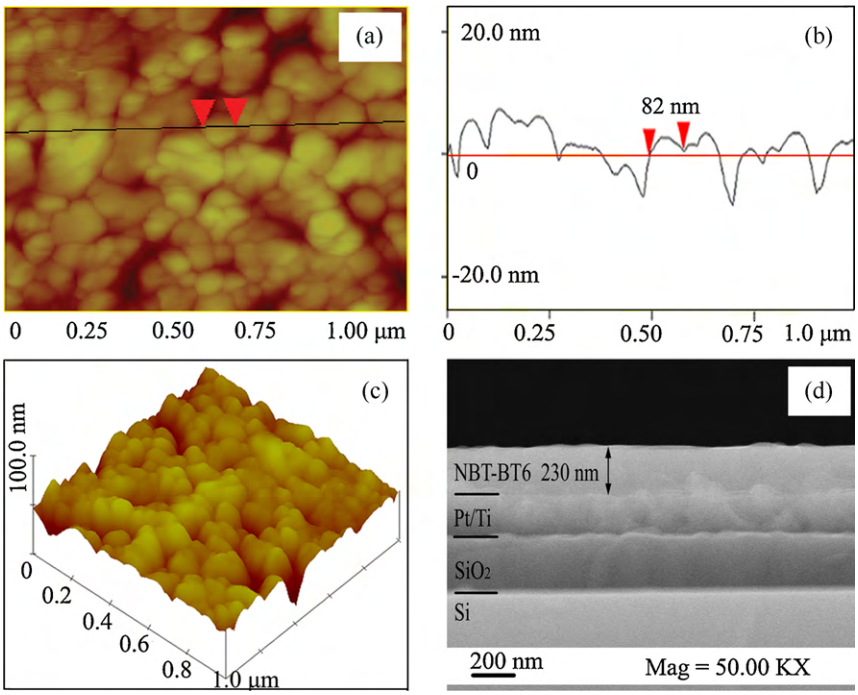

Fig. 3. (a) Surface morphology, (b) line profile analysis of morphology, and (c) three-dimensional image measured by AFM. (d) Cross-sectional FE-SEM micrograph.

crystallites, occurring for annealing temperature about 750 °C. The XRD pattern of NBT–BT6 thin film is given in Fig. 2(a). According to the Scherrer formulae $L = 0.9\lambda/(B\cos\theta)$, the average crystallite size 28 nm can be calculated from XRD pattern, where L, λ, B and θ are the crystallite size, the wavelength of the Cu K_α radiation, the full width at half maximum (FWHM) of the diffraction peak, and the Prague diffraction angle, respectively. From the Fig. 2(a), it is easy to read that the thin film is of polycrystalline structure without any preferred orientation, and exhibits dominant ABO_3 perovskite phase and minor pyrochlore phase. It is consistent with the existences of pyrochlore phase for the NBT thin films reported [18,25,26]. Additionally, the crystallization of NBT powder starts at about 600 °C and is completed at 900 °C through evaporation and condensation processes [25], therefore there may be the pyrochlore phase in the NBT–BT6 thin film annealed at 750 °C. In order to eliminate the minor pyrochlore phase, one could introduce the excess of volatile Na and Bi for precursor solution [27] and anneal at an appropriate temperature in oxygen atmosphere after each layer of coating [18]. A typical EDS spectrum of the NBT–BT6 thin film is given in Fig. 2(b), and the Na, Bi, Ba, Ti, and O peaks, which originate from the thin film, are detected obviously. The chemical composition of the thin film is analyzed, and the atomic ratio of Na:Bi:Ba:Ti is 0.43:0.37:0.05:1.00. Taking instrumental error into consideration, the contents of Na, Ba and Ti are close to the stoichiometry of NBT–BT6, but the Bi content is relatively low due to the possible Bi loss during high temperature annealing. For ABO_3 perovskite structure, the volatilization of A-site element, e.g. Bi in $(Na_{0.5}Bi_{0.5})TiO_3$ based solid solutions, will result in the deficiency in A-site cation, and thereafter the generation of oxygen vacancies due to the valence balance [28].

The surface morphology, line profile analysis of morphology, and three-dimensional image in 1 μm × 1 μm area are given in Fig. 3(a)–(c) for NBT–BT6 thin film, respectively. From the Fig. 3(a), the crack-free thin film exhibits a smooth and homogeneous microstructure with a few intergranular porosities. As shown in Fig. 3(b), the grain size marked by two arrows, as an example, is 82 nm and the average grain size is approximately 85 nm. In the Fig. 3(c), the gains are spherical, and the root-mean-square value of surface roughness is about 5 nm. The cross-sectional micrograph and film thickness are illustrated in Fig. 3(d), and the multiple-layer structure is obviously composed of NBT–BT6 thin film, Pt/Ti bottom electrode, SiO_2 oxide layer, and Si substrate. The dense film is crucial for MEMS application, and the film thickness 230 nm implies that the thickness of a coating/drying cycle is about 30 nm.

The experimental P–E hysteresis loops of NBT–BT6 thin film are shown in Fig. 4(a). The P–E loops are not fully saturated under high electric field, and they are consistent with the P–E loops of the previous NBT–BT6 thin films [15,29]. The localized oxygen vacancies trapped at grain boundaries can pin domains and result in large leakage current and polarization degradation [30]. In order to correct the measured P–E loop, the experimental P–E loop measured under the applied voltage of 18 V and the corresponding pure ferroelectric switching P–E loop after compensation of capacitance and conductivity, using a modified model to simulate P–E loop [31], are also depicted in Fig. 4(b). In comparison with the experimental loop, the pure loop is more saturated under high electric field and is of stronger spontaneous polarization. From the pure loop, the remanent polarization $2P_r$ and coercive field E_c are 24 μC/cm^2 and 103 kV/cm under 782 kV/cm, respectively. The $2P_r$ is comparable to that of reported NBT–BT6 thin film (about 17 μC/cm^2 under 500 kV/cm) [29].

Fig. 5 presents dielectric constant ε_r and dielectric loss $\tan\delta$ vs frequency curves measured at room temperature for NBT–BT6 thin film. The typical values of dielectric constant and dielectric loss are 504 and 0.05 at 1 kHz, which are less than the previous results ($\varepsilon_r = 710$ and $\tan\delta = 0.08$ at 1 kHz) of NBT–BT6 thin film [15]. With the increase from 100 Hz to 100 kHz, the dielectric constant steadily decreases, and the dielectric loss slightly decreases at first, and then quickly increases. This phenomenon has been observed in many ferroelectric films [15,18], and the reasons may be the hopping of oxygen vacancies [30] and the extrinsic resonance behavior resulting from the microstructure deficiency [15].

A typical butterfly-shaped first cycle D–V curve (black) and the corresponding first cycle $d^*_{33} - V$ (blue) loop are described in Fig. 6. The shift of the intersection for the D–V curve toward positive voltage direction is due to the bottom electrode/ferroelectric

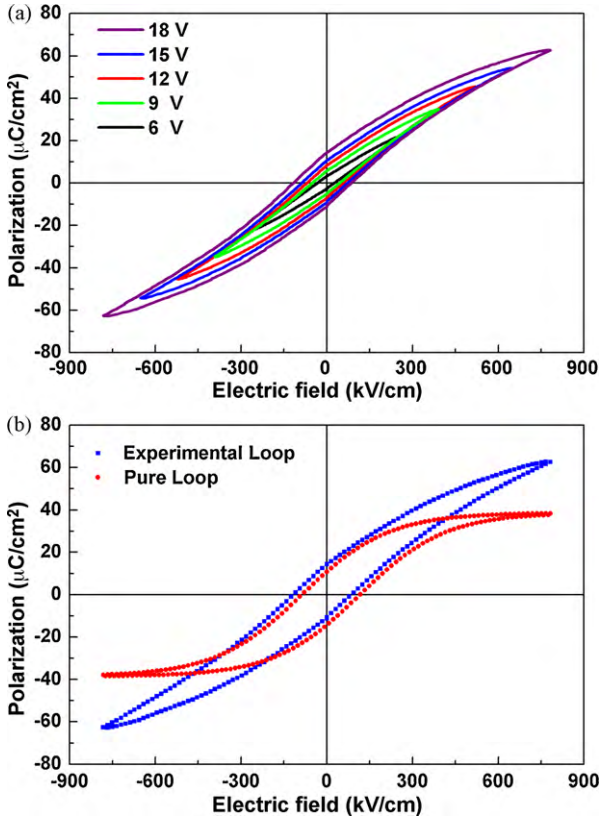

Fig. 4. (a) Experimental *P–E* hysteresis loops measured under applied voltage 6–18 V and 1 kHz by TF 2000 analyzer, (b) the experimental *P–E* loop measured under 18 V and the corresponding pure ferroelectric switching *P–E* loop after compensation of capacitance and conductivity.

interface and the asymmetry electrode structure [20], where the top conductive material is Rh while the bottom electrode is Pt. From the *D–V* curve, the piezoelectric displacement maximum is 982.9 pm at −8.7 V, and the corresponding electrically induced strain is as high as 0.39%. From the $d_{33}^* - V$ loop, the maximum value of d_{33}^* is estimated as 90.4 pm/V under the bipolar driving field of 391 kV/cm. For the 29 piezoelectric measurements, the average values of d_{33}^* and strain are 94 pm/V and 0.3%. The average value of d_{33}^* is comparable with the piezoelectric response of 80–100 pm/V for PZT thin films obtained by using a laser scanning vibrometer or a double-beam interferometer [32,33], however it is still much lower than 115–180 pm/V for NBT–BT6 ceramics measured

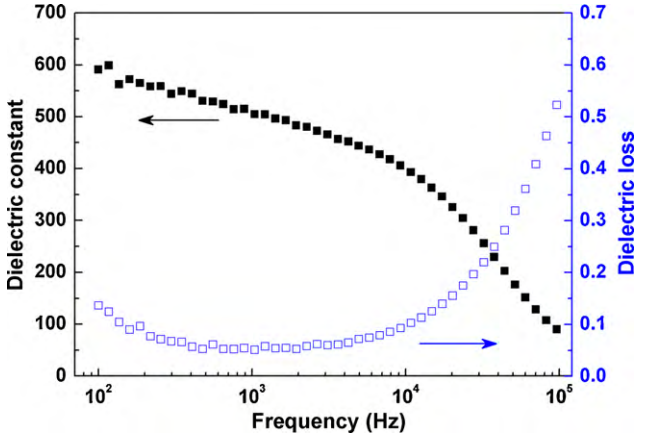

Fig. 5. Frequency dependences of the dielectric constant and dielectric loss at room temperature.

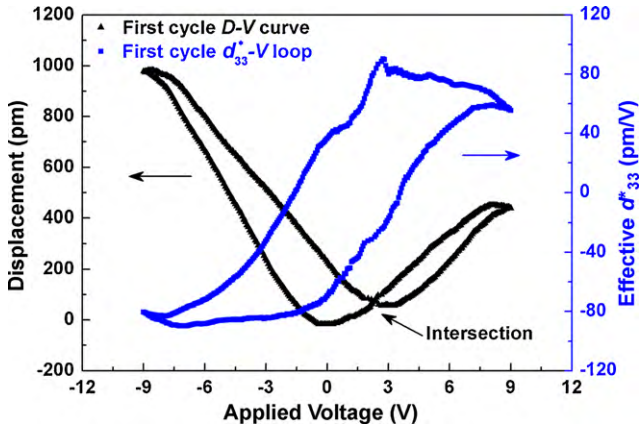

Fig. 6. The typical first cycle *D–V* curve (black) and the corresponding first cycle $d_{33}^* - V$ loop (blue) measured by SPM. (For interpretation of the references to color in this figure legend, the reader is referred to the web version of the article.)

by a resonance–antiresonance method or a quasistatic d_{33}-meter [6,12–14] because of clamping effect of the substrate, porosity, and small grain size [34]. In comparison with some lead-free piezoelectric thin films, the average value of d_{33}^* is higher than 40 pm/V for NBT thin film measured by using a combination of a SPM and a ferroelectric tester [35], 50 pm/V for $BaTiO_3$ thin film measured by using an AFM in combination with a lock-in amplifier [36], and 64 pm/V for $Bi_{0.5}(Na_{0.7}K_{0.2}Li_{0.1})_{0.5}TiO_3$ thin film measured by using an AFM in PFM mode [37]. Therefore the environment-friendly NBT–BT6 thin film may be considered as a promising alternate film material to PZT in piezoelectric devices such as MEMS, microactuators, transducers and micromotors.

The mechanisms concerning the dependence of the high piezoelectric performance for NBT–BT6 thin film with the composition near MPB are interpreted as follows. Firstly, electric field will be quite easy to tilt the polar vector of domain, and it may give rise to very strong piezoelectric activity [1]. Secondly, the increase in the number of possible spontaneous polarization direction may result in large coupling factors and high piezoelectric properties [38].

4. Conclusions

In summary, NBT–BT6 lead-free thin film is of the homogeneous and polycrystalline microstructure. The thin film shows the saturated pure ferroelectric switching *P–E* loop, and the values of $2P_r$ and E_c are 24 μC/cm² and 103 kV/cm under 782 kV/cm. The typical values of dielectric constant and dielectric loss are 504 and 0.05 at 1 kHz. The NBT–BT6 thin film exhibits high piezoelectric properties with the average d_{33}^* of 94 pm/V and the average strain of 0.3% under the bipolar driving field of 391 kV/cm, and the average d_{33}^* is comparable to those of PZT thin films and higher than those of some lead-free thin films reported. Therefore NBT–BT6 thin film is one of promising candidates for lead-free piezoelectric thin film applications.

Acknowledgements

This work was supported by NNSF of China (10825209, 50872117), Changjiang Scholar Incentive Program ([2009]17), Project of Hunan's Prestigious Fu-rong Scholar Award ([2007]362), Aid Program for Science and Technology Innovative Research Team in Higher Educational Institutions of Hunan Province, and Hunan Provincial Innovation Foundation for Postgraduate (CX2009B131).

References

[1] E. Cross, Nature (London) 432 (2004) 24–25.
[2] Y. Saito, H. Takao, T. Tani, T. Nonoyama, K. Takatori, T. Homma, T. Nagaya, M. Nakamura, Nature (London) 432 (2004) 84–87.
[3] G.A. Smolenskii, V.A. Isupov, A.I. Agranovskaya, N.N. Krainik, Sov. Phys. Solid State 2 (1961) 2651–2654.
[4] Q. Xu, D.P. Huang, M. Chen, W. Chen, H.X. Liu, B.H. Kim, J. Alloys Compd. 471 (2009) 310–316.
[5] M. Cernea, E. Andronescu, R. Radu, F. Fochi, C. Galassi, J. Alloys Compd. 490 (2010) 690–694.
[6] Q. Xu, X.L. Chen, W. Chen, B.H. Kim, S.L. Xu, M. Chen, J. Electroceram. 21 (2008) 617–620.
[7] Y. Wang, Z. Wang, H. Xu, D. Li, J. Alloys Compd. 484 (2009) 230–232.
[8] C. Zhou, X. Liu, W. Li, C. Yuan, J. Mater. Sci. Mater. El 21 (2010) 364–367.
[9] H. Zhang, S. Jiang, K. Kajiyoshi, J. Alloys Compd. 495 (2010) 173–180.
[10] W.C. Lee, C.Y. Huang, L.K. Tsao, Y.C. Wu, J. Alloys Compd. 492 (2010) 307–312.
[11] Y.M. Chiang, G.W. Farrey, A.N. Soukhojak, Appl. Phys. Lett. 73 (1998) 3683–3685.
[12] T. Takenaka, K.I. Maruyama, K. Sakata, Jpn. J. Appl. Phys. 30 (1991) 2236–2239.
[13] B.J. Chu, D.R. Chen, G.R. Li, Q.R. Yin, J. Eur. Ceram. Soc. 22 (2002) 2115–2121.
[14] Q. Xu, S. Chen, W. Chen, S. Wu, J. Lee, J. Zhou, H. Sun, Y. Li, J. Alloys Compd. 381 (2004) 221–225.
[15] Y. Guo, D. Akai, K. Sawada, M. Ishida, Solid State Sci. 10 (2008) 928–933.
[16] H.W. Cheng, X.J. Zhang, S.T. Zhang, Y. Feng, Y.F. Chen, Z.G. Liu, G.X. Cheng, Appl. Phys. Lett. 85 (2004) 2319–2321.
[17] N. Scarisoreanu, F. Craciun, V. Ion, S. Birjega, M. Dinescu, Appl. Surf. Sci. 254 (2007) 1292–1297.
[18] T. Yu, K.W. Kwok, H.L.W. Chan, Thin Solid Films 515 (2007) 3563–3566.
[19] A.L. Kholkin, E.K. Akdogan, A. Safari, P.F. Chauvy, N. Setter, J. Appl. Phys. 89 (2001) 8066–8073.
[20] H. Wen, X. Wang, C. Zhong, L. Shu, L. Li, Appl. Phys. Lett. 90 (2007) 202902.
[21] Y.C. Yang, C. Song, X.H. Wang, F. Zeng, F. Pan, Appl. Phys. Lett. 92 (2008) 012907.
[22] J.A. Christman, S.H. Kim, H. Maiwa, J.P. Maria, B.J. Rodriguez, A.I. Kingon, R.J. Nemanich, J. Appl. Phys. 87 (2000) 8031–8034.
[23] N. Balke, I. Bdikin, S.V. Kalinin, A.L. Kholkin, J. Am. Ceram. Soc. 92 (2009) 1629–1647.
[24] G. Braunstein, G.R. Paz-Pujalt, M.G. Mason, T. Blanton, C.L. Barnes, D. Margevich, J. Appl. Phys. 73 (1993) 961–970.
[25] C.Y. Kim, T. Sekino, Y. Yamamoto, K. Niihara, J. Sol–Gel Sci. Technol. 33 (2005) 307–314.
[26] J.P. Mercurio, P. Marchet, Integr. Ferroelectr. 61 (2004) 163–165.
[27] D. Alonso-Sanjosé, R. Jiménez, I. Bretos, M.L. Calzada, J. Am. Ceram. Soc. 92 (2009) 2218–2225.
[28] M. Zhu, H. Hu, N. Lei, Y. Hou, H. Yan, Appl. Phys. Lett. 94 (2009) 182901.
[29] Y. Guo, M. Li, W. Zhao, D. Akai, K. Sawada, M. Ishida, M. Gu, Thin Solid Films 517 (2009) 2974–2978.
[30] Z.H. Zhou, J.M. Xue, W.Z. Li, J. Wang, H. Zhu, J.M. Miao, Appl. Phys. Lett. 85 (2004) 804–806.
[31] R. Jiménez, C. Alemany, M.L. Calzada, A. González, J. Ricote, J. Mendiola, Appl. Phys. A 75 (2002) 607–615.
[32] W. Gong, J.F. Li, X.C. Chu, Z.L. Gui, L.T. Li, Acta Mater. 52 (2004) 2787–2793.
[33] S. Hiboux, P. Muralt, N. Setter, Mater. Res. Soc. Symp. Proc. 596 (2000) 499–504.
[34] H. Zhang, S. Jiang, Y. Zeng, Appl. Phys. Lett. 92 (2008) 152901.
[35] T. Hayashi, T. Kogure, W. Sakamoto, Proc. 16th IEEE Int. Symp. Applications of Ferroelectrics, 2007, pp. 104–105.
[36] Y. Guo, K. Suzuki, K. Nishizawa, T. Miki, K. Kato, Acta Mater. 54 (2006) 3893–3898.
[37] D.Y. Wang, D.M. Lin, K.S. Wong, K.W. Kwok, J.Y. Dai, H.L.W. Chan, Appl. Phys. Lett. 92 (2008) 222909.
[38] Y. Hosono, K. Harada, Y. Yamashita, Jpn. J. Appl. Phys. 40 (2001) 5722–5726.